ARCHIVES OF ELECTRICAL ENGINEERING VOL. 72(1), pp. 211–228 (2023)

DOI 10.24425/aee.2023.143698

A comparative study based on proportional integral and backstepping controllers for doubly fed induction generator used in wind energy conversion system

YOUSSEF MOUMANI ✉, ABDESLAM JABAL LAAFOU, ABDESSALAM AIT MADI

Advanced Systems Engineering Laboratory,
National School of Applied Sciences, Ibn Tofail University
Kenitra, Morocco

e-mail: {✉youssef.moumani/abdeslam.jaballaafou/abdessalam.aitmadi@uit.ac.ma}

(Received: 11.04.2021, revised: 09.11.2022)

Abstract: This paper presents a comparative study between the conventional PI (Proportional Integral) and backstepping controllers applied to the DFIG (Doubly Fed Induction Generator) used in WECS (Wind Energy Conversion System). These two different control strategies proposed in this work are developed to control the active and reactive power of the DFIG on the one hand, and to maintain the DC-link voltage constant for the inverting function on the other hand. This is ensured by generating control signals for two power electronic converters, RSC (Rotor Side Converter) and GSC (Grid Side Converter). In order to optimise the power production in the WT (Wind Turbine), an MPPT (Maximum Power Point Tracking) algorithm is applied along with each control technique. To simulate the effectiveness of the proposed controllers, MATLAB/Simulink Software is used, and the obtained results are analysed and discussed to compare PI and backstepping controllers in terms of robustness against wind speed variations and tracking performance in dynamic and steady states.

Key words: backstepping control, control, DFIG, GSC, MPPT, PI, RSC, wind turbine

1. Introduction

The huge increase in energy needs and demands around the world forces the international community to invest more in renewable energy sources [1]. This shift towards renewable energies makes wind energy become one of the fastest growing and most reliable renewable energy technologies, especially in the last few decades [2, 3]. In this context many studies have been

conducted in attempt to enhance the efficiency of the wind turbines as well as to improve the quality of the energy produced.

Most of WTs (Wind Turbines) that are installed nowadays are based on variable speed generators, the DFIG (Doubly Fed Induction Generator) [4, 5]. It is the most used generator, especially in conventional gear-driven WT systems due to its several advantages such as the small size of the converters needed for power control as they are penetrated only by a fraction of the rated power. It's also more useful to control power in case of high wind speed for protection reasons. Another advantage is that the DFIG does not need either a reactive power compensator or a soft starter because its structure offers the possibility to control reactive power exchanged between the turbine and the grid through two electronic converters, the RSC (Rotor Side Converter) and GSC (Grid Side Converter) [6].

The most typical topology design of the WECS (Wind Energy Conversion System) is shown in Fig. 1, where the turbine shaft drives the rotor of the DFIG through the gear box system. The stator windings are directly connected to the power grid whereas the rotor windings are connected to the grid through back-to-back power electronic converters, the RSC and GSC, with a DC-link capacitor in between to keep the voltage constant for the inverting function [4, 6].

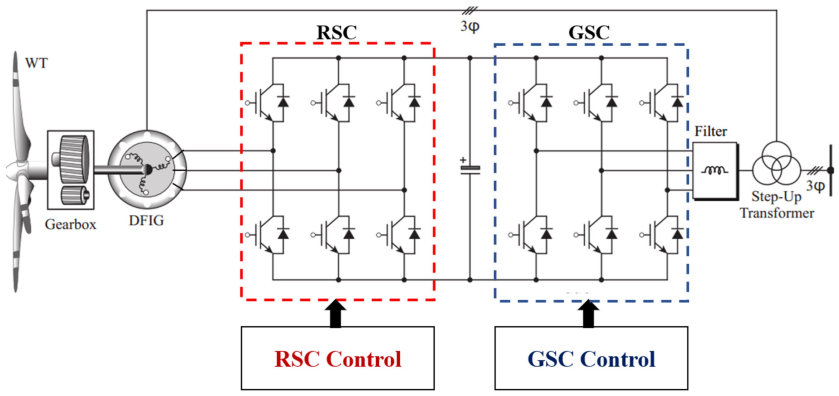

Fig. 1. Block diagram of WECS based on DFIG

In order to maximise the power captured by the WT, the control strategy of the DFIG has become the issue and interest of recent studies as highlighted by F. Mohammadi *et al.* [7].

In a grid connected wind turbine, power fluctuations have a negative effect on the quality of energy produced. To deal with this issue some studies propose an optimal control method in order to optimise the capacity and reliability of storage devices [8]. The use of emergency power transmission lines is also proposed despite the economic uncertainties [9].

The most popular strategy adopted to control the WT is the conventional PI (Proportional Integral) but the non-linearity of the DFIG makes it difficult to achieve satisfying performances in terms of reference tracking and speed response. That is why we propose a non-linear controller based on a backstepping approach to be applied to both converters, to consider the useful non-linearities of the system [10].

Furthermore, a detailed comparative study between the PI and backstepping controllers will be presented in this article to test their performances in terms of robustness against wind speed variations and reference tracking in dynamic and steady states.

This paper is organised as follows:

In section 2, the related work is given. Section 3 gives the dynamic model of the WECS including the DFIG. A PI controller is designed in section 4, a backstepping controller is developed in section 5. Simulation results are presented and discussed in section 6. Finally, section 7 contains the conclusion.

2. Related work

The literature review shows that there is a series of studies that contributed to the design of PI and backstepping control strategies applied to the DFIG driven by the WT.

El Mouhi *et al*. [11] proposed an active and reactive power control of the DFIG used in the WECS using the PI controller and backstepping. This study focused on the difference between PI and backstepping controllers in terms of dynamic response.

M. Nadour *et al*. [12] proposed a comparative analysis between PI and backstepping control strategies of the DFIG driven by the WT. This study shed the light on the comparison in terms of parametric variations.

S. Mensou *et al*. [13] proposed the backstepping controller for a Variable Wind Speed Energy Conversion System based on the DFIG. In this study, the backstepping control performance has been evaluated against random speed variations.

A.J. Laafou proposed the dynamic control of the DFIG used in wind power production, based on a PI regulator. In this work the performances of the PI controller are simulated and tested [11].

Y. Moumani *et al*. [15] proposed modeling and backstepping control of the DFIG used in Wind Energy Conversion Systems. It focused on the evaluation of the proposed backstepping controller in terms of reference tracking and robustness against wind speed variations.

B. Bossoufi *et al*. [17] proposed the backstepping adaptive control of the DFIG for variable speed WTs. This study presents a nonlinear backstepping controller that is designed using an adaptive pole placement strategy applied to WTs.

In this work we tried to combine all these studies mentioned to highlight the performances of both PI and backstepping controllers, in terms of robustness against wind speed variations and reference tracking in dynamic and steady states.

3. Wind turbine and DFIG modelling

As shown earlier in Fig. 1, the wind energy conversion system considered in our study is composed of a three-bladed horizontal-axis turbine and a DFIG generator, separated by a gear box system for speed adaptation.

In this adopted topology, the stator windings are directly connected to the grid and the rotor is connected to the grid through two power electronic converters, the RSC and GSC.

The model of both the mechanical and electrical parts is given below.

3.1. Turbine model

The aerodynamic power of a turbine is written by Eq. (1) according to O. Barambones [14].

$$P_{\text{aero}} = C_p(\lambda, \beta)\frac{1}{2}\rho\pi R^2 v^3, \tag{1}$$

where C_p is the power coefficient that depends on the tip speed ratio λ and the pitch angle β. R is the blade radius and v is the wind speed.

The tip speed ratio λ is calculated by Eq. (2) [14].

$$\lambda = \frac{R\Omega_t}{v}, \tag{2}$$

where Ω_t is the rotational speed of a turbine.

The expression of the power coefficient C_p of the turbine considered in this work is given by the following equation, (3).

$$C_p = 0.5176\left(\frac{116}{\lambda_i} - 0.4\beta - 5\right)e^{-\frac{21}{\lambda_i}} + 0.068\lambda, \tag{3}$$

where:

$$\lambda_i = \frac{1}{\lambda + 0.08\beta} - \frac{0.035}{1+\beta^3}. \tag{4}$$

3.2. Gearbox model

The gear box system is modelled by the two equations bellow [15].

$$\begin{cases} \Omega_m = G \cdot \Omega_t \\ T_t = G \cdot T_m \end{cases}, \tag{5}$$

where: G is the gear ratio, Ω_m and T_m are, respectively, the mechanical speed and the torque of the generator, Ω_t and T_t are, respectively, the mechanical speed and the torque of the turbine.

The dynamic equation of the generator speed is given by the following equation, (6).

$$J\frac{\mathrm{d}\Omega_m}{\mathrm{d}t} = T_m - T_{em} - f\Omega_m, \tag{6}$$

where: T_{em} is the electromagnetic torque, $f\Omega_m$ is the torque of viscous friction and J is the moment of inertia.

3.3. DFIG Model

The dynamic model of the DFIG, adopted in this work, was built based on equations in the *dq* reference frame as indicated in the literature [10–12].

The rotor and stator voltages are illustrated by Eq. (7a) and the fluxes are given in the dq reference by Eq. (7b).

$$\begin{cases} V_{sd} = R_s i_{sd} + \dfrac{\mathrm{d}\phi_{sd}}{\mathrm{d}t} - \omega_s \phi_{sq} \\ V_{sq} = R_s i_{sq} + \dfrac{\mathrm{d}\phi_{sq}}{\mathrm{d}t} + \omega_s \phi_{sd} \\ V_{rd} = R_s i_{rd} + \dfrac{\mathrm{d}\phi_{rd}}{\mathrm{d}t} - \omega_r \phi_{rq} \\ V_{rq} = R_s i_{rq} + \dfrac{\mathrm{d}\phi_{rq}}{\mathrm{d}t} + \omega_r \phi_{rd} \end{cases}, \tag{7a}$$

$$\begin{cases} \phi_{sd} = L_s i_{sd} + L_m i_{rd} \\ \phi_{sq} = L_s i_{sq} + L_m i_{rq} \\ \phi_{rd} = L_r i_{rd} + L_m i_{sd} \\ \phi_{rq} = L_r i_{rq} + L_m i_{sq} \end{cases}. \tag{7b}$$

The active and reactive power are givens by the following equations, (8) and (9).

$$\begin{cases} P_s = V_{sd} i_{sd} + V_{sq} i_{sq} \\ Q_s = V_{sq} i_{sd} + V_{sd} i_{sq} \\ P_r = V_{rd} i_{rd} + V_{rq} i_{rq} \\ Q_r = V_{rq} i_{rd} + V_{rd} i_{rq} \end{cases}. \tag{8}$$

The electromagnetic torque T_{em} is given by Eq. (9).

$$T_{em} = p \frac{L_m}{L_s} \left(\phi_{sq} i_{rd} - \phi_{sd} i_{rq} \right). \tag{9}$$

In order to achieve a vector control of active and reactive power, the stator field vector is oriented along the d-axis ($\phi_{sd} = \phi_s$ and $\phi_{sq} = 0$) [11, 13].

For simplification reasons, the stator resistance is considered negligible, $R_s = 0$.

Therefore, previous Eq. (7a) become Eq. (10).

$$\begin{cases} V_{sd} = 0 \\ V_{sq} = \omega_s \phi_s \\ V_{rd} = R_r i_{rd} + L_r \sigma \dfrac{\mathrm{d}i_{rd}}{\mathrm{d}t} - g \omega_s L_r i_{rq} \\ V_{rq} = R_r i_{rq} + L_r \sigma \dfrac{\mathrm{d}i_{rq}}{\mathrm{d}t} - g \omega_s L_r i_{rq} + g \omega_s \dfrac{V_s L_m}{L_s \omega_s} \end{cases}, \tag{10}$$

where $\sigma = 1 - \dfrac{L_m^2}{L_s L_r}$.

Therefore, the simplified expressions of the stator active and reactive power are given by Eq. (11).

$$\begin{cases} P_s = -\dfrac{V_s L_m}{L_s} i_{rq} \\ Q_s = -\dfrac{V_s L_m}{L_s} i_{rd} + \dfrac{V_s^2}{L_s \omega_s} \end{cases}. \tag{11}$$

Thus, the electromagnetic torque is given by Eq. (12).

$$T_{em} = -p\frac{L_m}{L_s}\phi_s i_{rq}\,. \tag{12}$$

4. PI controller design

In order to apply the PI control strategy for the RSC, the DFIG's model adopted previously in section 2 will be considered.

Considering the previous equations, (11) and (12), one can see that the control of the electromagnetic torque T_{em} is ensured by the quadrature component of the rotor current i_{rq} and the reactive power Q_s is controlled by the direct component i_{rd} in the dq reference frame.

Both the active power P_s or the electromagnetic torque T_{em} can be controlled. In both cases their references are obtained from the MPPT algorithm to guarantee the optimisation of the power captured by the WT.

The schematic diagram of the PI controller applied to the RSC is illustrated in Fig. 2.

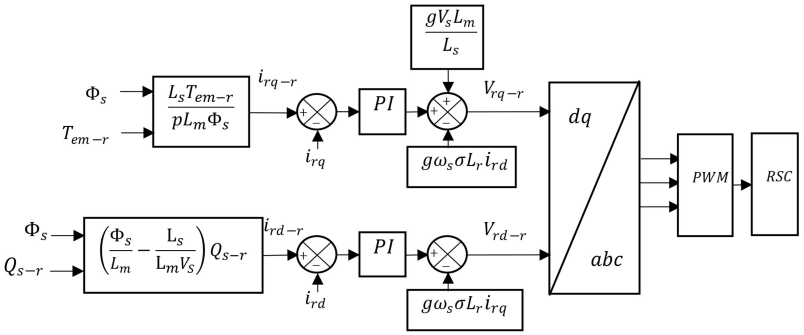

Fig. 2. Schematic diagram of the PI controller for RSC

The parameters of each PI controller applied are obtained based on the transfer function of the considered block. These parameters are determined using the pole compensation method in the closed loop. The structure of the PI controller including the transfer function of the rotor currents are given in Fig. 3.

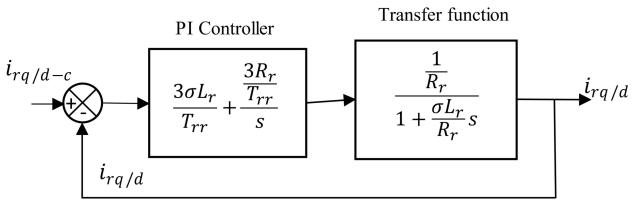

Fig. 3. Block diagram of PI controller of RSC

There, T_{rr} is the settling time of the rotor currents, and the parameters of the controller are chosen, as mentioned, by A.J. Laafou *et al.* [19].

In the same way, the structure of the schematic diagram of the PI controller for the GSC is illustrated in Fig. 4. Furthermore, the DC-link and grid current PI controllers applied to the GSC are illustrated in Fig. 5. As seen in the same figure, these two PI controllers are applied to the grid side, respectively, after developing the RL filter and DC link capacitor models.

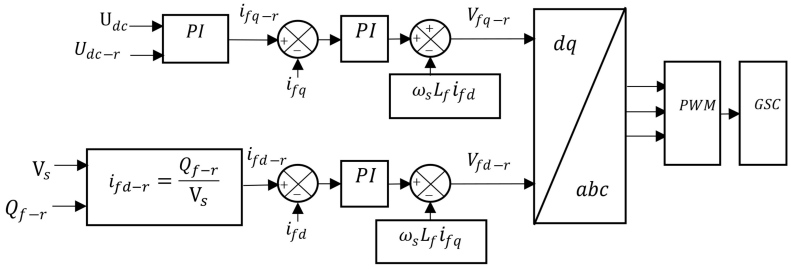

Fig. 4. Schematic diagram of PI control of GSC

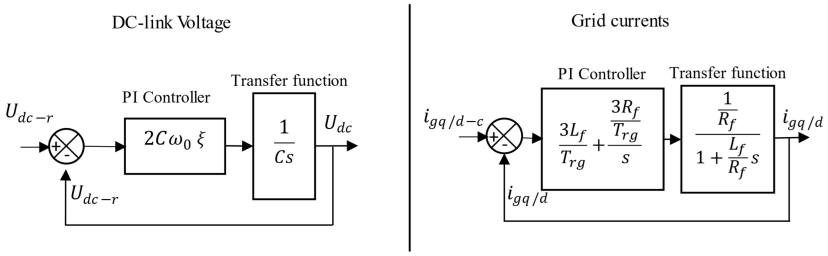

Fig. 5. PI controllers of the grid currents and DC-link voltage

Here, T_{rg} is the settling time of grid currents, and the parameters of the controller are chosen as in [19].

The parameters of this controller can be simplified as follows:

For rotor currents
$$K_p^r = \frac{3\sigma L_r}{T_{rr}}, \qquad K_i^r = \frac{3R_r}{T_{rr}}. \tag{13}$$

For grid currents
$$K_p^r = \frac{3L_f}{T_{rg}}, \qquad K_i^r = \frac{3R_f}{T_{rg}}. \tag{14}$$

For DC link voltage
$$K_p^{dc} = 2C\omega_0\xi, \qquad K_i^{dc} = \omega_0^2 C = \frac{3}{\xi . T_{rdc}}. \tag{15}$$

The setting values of these parameters are given in the Appendix.

5. Backstepping controller design

5.1. RSC control

To design the backstepping controller for the RSC, the stator active and reactive power P_s and Q_s are provided by the following equations, (16) and (17), which have been derived from the DFIG model.

Active power

$$\begin{cases} P_s = -\dfrac{V_s L_m}{L_s} i_{rq} \\ \dot{i}_{rq} = \dfrac{1}{\sigma L_r}\left(V_{rq} - R_r i_{rq} - \sigma L_r \omega_r i_{rd} - g\dfrac{V_s L_m}{L_s}\right) \end{cases}, \tag{16}$$

Reactive power

$$\begin{cases} Q_s = -\dfrac{V_s L_m}{L_s} i_{rd} + \dfrac{V_s^2}{L_s \omega_s} \\ \dot{i}_{rd} = \dfrac{1}{\sigma L_r}\left(V_{rd} - R_r i_{rd} - \sigma L_r \omega_r i_{rq}\right) \end{cases}. \tag{17}$$

These types of stator power are controlled by the rotor currents $\dot{i}_{rq}$ and $\dot{i}_{rd}$ with an intermediate virtual control v_{rq} and v_{rd}. Their reference values are determined following the recursive and sequential steps of backstepping control strategy based on the Lyapunov function [20]. Consequently, in order to achieve the stability of the system, the design of the backstepping controller can be carried out following two steps, as seen below. The current references (see Eq. 18) and the control voltages (see Eq. (24)) are computed, respectively, in the first and second step.

Step 1: Computation of current references:

Tracking errors:

$$\begin{cases} \varepsilon_1 = P_{s-c} - P_s \\ \varepsilon_3 = Q_{s-c} - Q_s \end{cases} \Longrightarrow \begin{cases} \dot{\varepsilon}_1 = \dot{P}_{s-c} - \dot{P}_s \\ \dot{\varepsilon}_3 = \dot{Q}_{s-c} - \dot{Q}_s \end{cases}. \tag{18}$$

Lyapunov functions:

$$V_1 = \frac{1}{2}\varepsilon_1^2, \quad V_3 = \frac{1}{2}\varepsilon_3^2. \tag{19}$$

Derivatives of Lyapunov functions:

$$\begin{cases} \dot{V}_1 = \varepsilon_1 \dot{\varepsilon}_1 = \varepsilon_1 \left[\dot{P}_{s-c} - A_1\left(V_{rq} - R_r i_{rq} - A_2 i_{rd} - A_3\right)\right] \\ \dot{V}_3 = \varepsilon_3 \dot{\varepsilon}_3 = \varepsilon_3 \left[\dot{Q}_{s-c} - A_1\left(V_{rd} - R_r i_{rd} + A_2 i_{rq}\right)\right] \end{cases}, \tag{20}$$

where:

$$A_1 = \frac{V_s L_m}{L_s \sigma L_r}, \quad A_2 = \sigma L_r \omega_r, \quad A_3 = g\frac{V_s L_m}{L_s}.$$

Rotor currents as virtual commands:

$$\begin{aligned} i_{rq-c} &= \frac{1}{A_1 R_r}\left[\dot{P}_{s-c} + c_1 \varepsilon_1\right] - \frac{1}{R_r}\left(V_{rq} - A_2 i_{rd} - A_3\right), \\ i_{rd-c} &= \frac{1}{A_1 R_r}\left[\dot{Q}_{s-c} + c_3 \varepsilon_3\right] - \frac{1}{R_r}\left(V_{rd} + A_2 i_{rq}\right). \end{aligned} \tag{21}$$

Step 2: Computation of control voltages:
Tracking errors:

$$\begin{cases} \varepsilon_2 = i_{rq-c} - i_{rq} \\ \varepsilon_4 = i_{rd-c} - i_{rd} \end{cases} \Longrightarrow \begin{cases} \dot{\varepsilon}_2 = \dot{i}_{rq-c} - \dot{i}_{rq} \\ \dot{\varepsilon}_4 = \dot{i}_{rd-c} - \dot{i}_{rd} \end{cases}. \tag{22}$$

Lyapunov functions:

$$V_2 = \frac{1}{2}\varepsilon_1^2 + \frac{1}{2}\varepsilon_2^2, \quad V_4 = \frac{1}{2}\varepsilon_3^2 + \frac{1}{2}\varepsilon_4^2. \tag{23}$$

Derivatives Lyapunov functions:

$$\begin{cases} \dot{V}_2 = \varepsilon_1\dot{\varepsilon}_1 + \varepsilon_2\dot{\varepsilon}_2 \\ \dot{V}_4 = \varepsilon_3\dot{\varepsilon}_3 + \varepsilon_4\dot{\varepsilon}_4 \end{cases}. \tag{24}$$

Therefore:

$$\begin{cases} \dot{V}_2 = \varepsilon_1 \left[\dot{P}_{s-c} - A_1 \left(V_{rq} - R_r \left(i_{rq-c} - \varepsilon_2\right) - A_2 i_{rd} - A_3\right)\right] \\ \qquad + \ \varepsilon_2 \left[\dot{i}_{rq-c} - \dfrac{1}{\sigma L_r}\left(V_{rq} - R_r \left(i_{rq-c} - \varepsilon_2\right) - A_2 i_{rd} - A_3\right)\right] \\ \dot{V}_4 = \varepsilon_3 \left[\dot{Q}_{s-c} - A_1 \left(V_{rd} - R_r \left(i_{rd-c} - \varepsilon_4\right) + A_2 i_{rq}\right)\right] \\ \qquad + \ \varepsilon_4 \left[\dot{i}_{rd-c} - A_1 \left(V_{rd} - R_r \left(i_{rd-c} - \varepsilon_4\right) - A_2 i_{rq}\right)\right] \end{cases}. \tag{25}$$

Finally, we will have to choose the references of rotor voltages as the actually accessible commands. Their reference values should guarantee that the derivatives of Lyapunov functions are negative as expressed by Eq. (26).

$$\dot{V}_2 = -c_1\varepsilon_1^2 - c_2\varepsilon_2^2 < 0, \quad \dot{V}_4 = -c_3\varepsilon_3^2 - c_4\varepsilon_4^2 < 0, \tag{26}$$

where c_1, c_2, c_3 and c_4 are positive parameters that we must choose properly to ensure asymptotic convergence stability according to the Lyapunov theory [17].

In our simulation model we chose them as, $c_1 = 80\,000$, $c_2 = 5\,000$, $c_3 = 9\,000$ and $c_4 = 6\,000$ [17].

Therefore, the control voltages are given by Eq. (27).

$$\begin{cases} V_{rq-c} = \dfrac{1}{\sigma L_r}\left[-c_2\varepsilon_2 - \dot{i}_{rq-c} + A_1 R_r \varepsilon_1\right] + B_1 \\ V_{rd-c} = \dfrac{1}{\sigma L_r}\left[-c_4\varepsilon_4 - \dot{i}_{rd-c} + A_1 R_r \varepsilon_3\right] + B_2 \end{cases}, \tag{27}$$

where:

$$B_1 = -R_r \left(i_{rq-c} - \varepsilon_2\right) - A_2 i_{rd} - A_3 \quad \text{and} \quad B_2 = -R_r \left(i_{rd-c} - \varepsilon_4\right) + A_2 i_{rq}\,.$$

The block diagram of the backstepping controller applied to the RSC is presented in Fig. 6. In this diagram all the steps, previously mentioned, that are required to turn out the control law of the rotor voltages are illustrated.

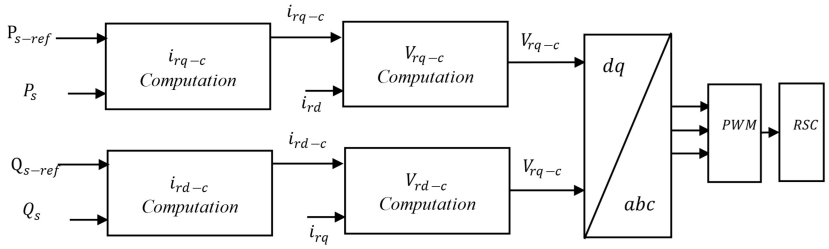

Fig. 6. Backstepping control diagram applied to the RSC

5.2. GSC control

For the control of the GSC, we consider the model of the RL filter, which is defined by equations of the rotor active and reactive power, (28) and (29).

$$\text{Active power} \qquad \begin{cases} \dot{P}_f = \dfrac{V_s}{L_f}\left(V_{fq} - R_f i_{fq} - L_f \omega_s i_{fd} - V_s\right) \\ \dot{i}_{fq} = \dfrac{1}{L_f}\left(V_{fq} - R_f i_{fq} - L_f \omega_s i_{fd} - V_s\right) \end{cases}, \tag{28}$$

$$\text{Reactive power} \qquad \begin{cases} \dot{Q}_f = \dfrac{V_s}{L_f}\left(V_{fd} - R_f i_{fd} - L_f \omega_s i_{fq} - V_s\right) \\ \dot{i}_{fd} = \dfrac{1}{L_f}\left(V_{fd} - R_f i_{fd} - L_f \omega_s i_{fq} - V_s\right) \end{cases}. \tag{29}$$

By following the same backstepping strategy detailed earlier in RSC control according to the use of Lyapunov functions, the expressions of the filter current reference Eq. (30) of i_{fq} and i_{fd} are given in the first step, while voltage reference Eq. (31), V_{fd} and V_{fq}, are given in the second step.

Therefore:

$$\text{Grid current references:} \qquad \begin{cases} i_{fq-c} = \dfrac{1}{R_f}\left[\dfrac{L_f}{V_s}\left(\dot{P}_{f-c} + k_1\varepsilon_1\right) + \left(V_{fq} - L_f\omega_s i_{fd} - V_s\right)\right] \\ i_{fd-c} = \dfrac{1}{R_f}\left[\dfrac{L_f}{V_s}\left(\dot{Q}_{s-c} + k_3\varepsilon_3\right) + \left(V_{fd} - L_f\omega_s i_{fq}\right)\right] \end{cases}, \tag{30}$$

$$\text{Voltages references:} \qquad \begin{cases} V_{fq-c} = L_f\left(-k_2\varepsilon_2 - \dot{i}_{fq-c} + \dfrac{V_s}{L_f}\varepsilon_1\right) - \left(R_f i_{fq} + L_f\omega_s i_{fd} + V_s\right) \\ V_{fd-c} = L_f\left(-k_4\varepsilon_4 - \dot{i}_{fd-c} + \dfrac{V_s}{L_f}\varepsilon_3\right) - \left(R_f i_{fd} - L_f\omega_s i_{fq}\right) \end{cases}. \tag{31}$$

In the same way as PI controllers for the RSC, the parameters k_1, k_2, k_3 and k_4 are positive parameters chosen properly to guarantee the asymptotic convergence stability according to the Lyapunov theory. According to Y. Moumani *et al.* [17], they are chosen in this proposed model to be

$$k_1 = 10\,000, \quad k_2 = 80\,000, \quad k_3 = 20\,000 \quad \text{and} \quad k_4 = 6\,000.$$

Based on Eqs. (28) and (29), the block diagram of the backstepping controller applied to the GSC is given in Fig. 7.

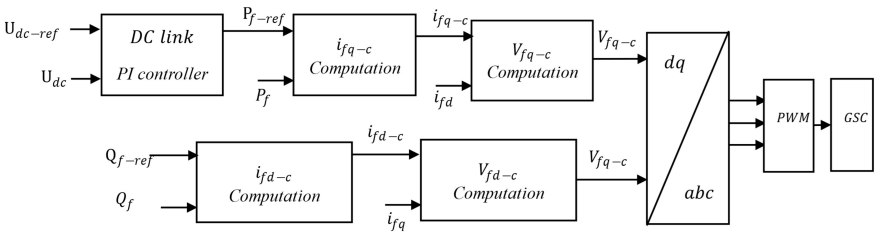

Fig. 7. Block diagram of backstepping controller applied to the GSC

6. Simulation results

To validate the performance of the proposed PI and backstepping controllers, MATLAB/ Simulink software has been used to build the model of the entire WECS including the turbine and the DFIG.

After designing the two controllers, the simulation scenario adopted is based on a wind speed profile as a signal of sudden changes in wind speed, as illustrated in Fig. 8 allows one to test tracking speed as well as tracking error in both transient and steady states.

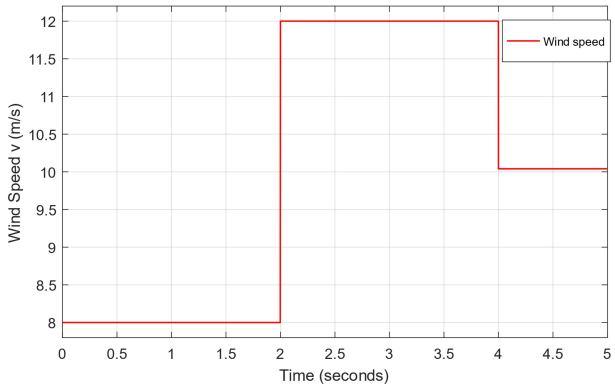

Fig. 8. Form of applied wind speed profile

The obtained results for the stator active and reactive power are presented respectively in Fig. 9 and Fig. 10. From these figures, one can see obviously that the outputs P_s and Q_s converge perfectly to their references when there is a random sudden change of wind speed. The value of P_s is negative because DFIG works as a generator.

The active power P_s converges to its reference value $P_{s-\mathrm{ref}}$ determined by an MPPT algorithm and the reactive power is kept at zero to ensure a unitary power factor [21]. This means that all the tracking errors converge to zero. That proves the effectiveness of the two controllers, but

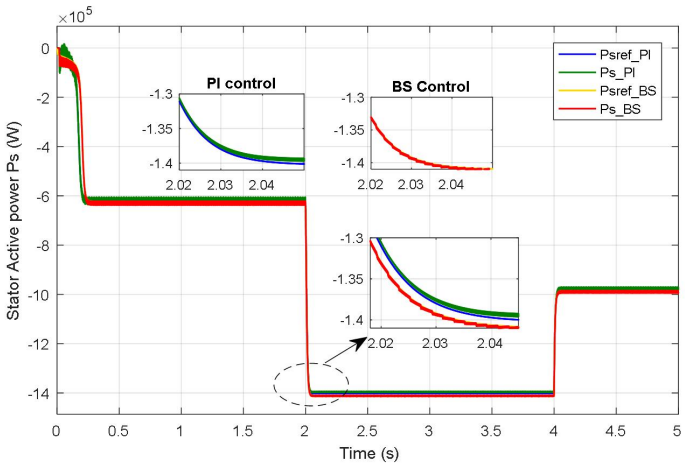

Fig. 9. Stator active power for PI and BS control

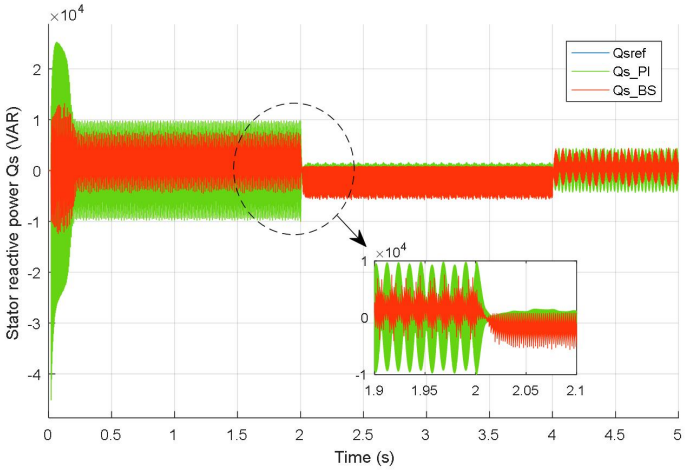

Fig. 10. Stator reactive power for PI and BS control

backstepping is quite more effective than PI when it comes to error cancellation in both transient and steady states.

Fig. 11 shows the evolution of the power factor C_p that depends on wind speed. In this figure, one can see that the power coefficient is kept at its optimal value despite the disturbance caused by the sudden changes in wind speed. The principal observed advantage here is that the backstepping controller response is much faster than that of the PI controller.

Fig. 12, which illustrates the DC link voltage for both PI and backstepping controllers, shows that there is overshooting in the PI control strategy, the voltage value exceeds its reference value while trying to stabilise against wind speed changes.

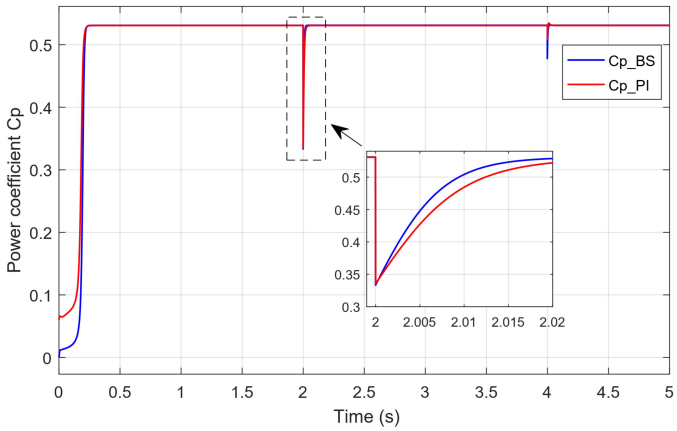

Fig. 11. Power coefficient C_p

Apparently, the same previous observations regarding the settling time are also noticed in Fig. 12. The voltage U_{dc} follows its reference with a very small settling time which means that is much faster compared to PI.

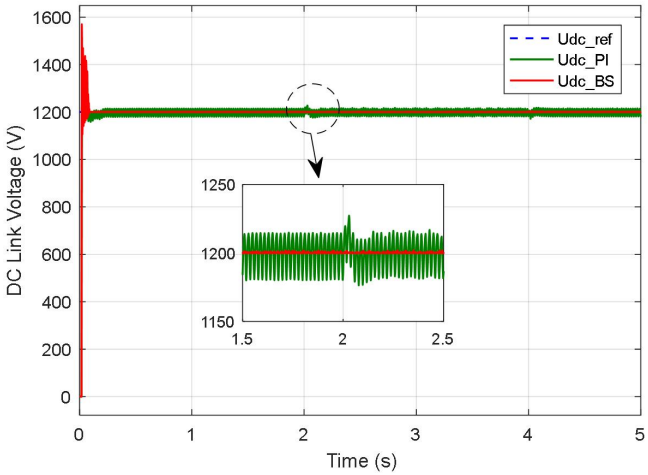

Fig. 12. DC-Link voltage U_{dc}

Figures 13 and 14 present, respectively, the rotor active and reactive power for both PI and backstepping controllers. From Fig. 13 one can notices that the power P_f is negative between 2 s and 4 s. It means that the DFIG works in hypersynchronous mode, which is obvious since the rotor speed exceeds its nominal value. Whereas the reactive power of the rotor is kept at zero, to ensure a unitary power factor, as illustrated by Fig. 14.

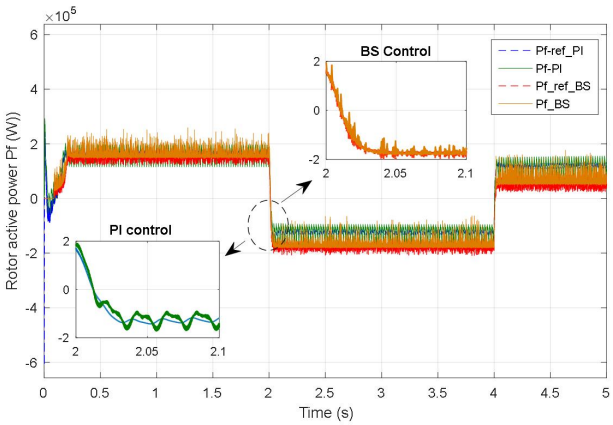

Fig. 13. Rotor active power P_f

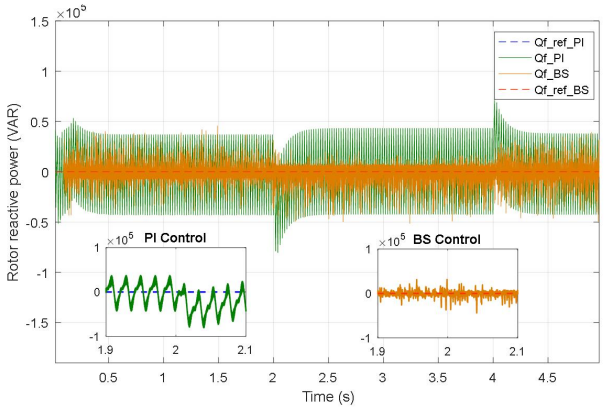

Fig. 14. Rotor reactive power Q_f

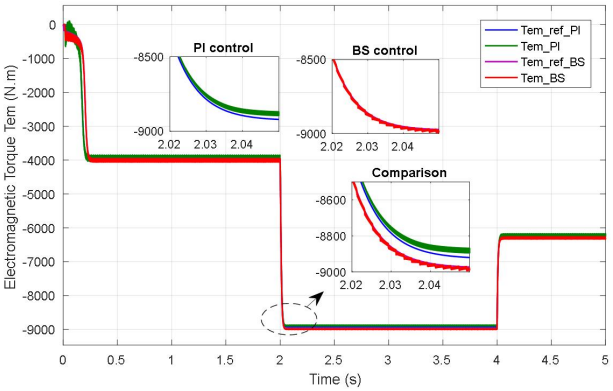

Fig. 15. Electromagnetic torque T_{em} (N·m)

For both controls, the electromagnetic torque T_{em} is illustrated by the following Figure 15, it has exactly the same form of active power which affirms the same differences discussed earlier between PI and backstepping.

7. Conclusion

In this paper a comparative study between two control strategies was given. The studied controllers are the conventional PI control and an advanced non-linear approach known as backstepping control. These two strategies, to control a WT-driven DFIG, are applied to two converters, the RSC and GSC, leading to the optimization of the power captured by the WT.

The obtained results carried out from this study have proved that both controllers show quite satisfying performances, but the backstepping technique is more effective in terms of robustness against disturbances such as wind speed variations.

Moreover, the non-linearity of the backstepping makes the system more stable and much faster than its competitor due to its short settling time which proves its capability to cancel the tracking errors in a very short time.

However, the simplicity and the low cost of the classical PI controller make it still the most employed controller compared to the backstepping controller which is more complex, and more sensors are needed for its implementation.

In future work, a hardware implementation, as well as a further study, should be carried on in order to test the performances of the proposed controllers against voltage dips expected in the terminals of the wind power system.

Nomenclature

P_{aero} : The aerodynamic power of wind turbine (W)
T_t : Wind turbine torque (N.m)
v : Wind speed (m/s)
R : Blade radius (m)
λ : Tip speed ratio
G : Gearbox ratio
Ω_m : mechanical speed of the generator (rad/s)
T_m : mechanical torque of the generator (N.m)
f : Damping coefficient
p : number of pair poles
J : Moment of inertia
T_{em} : Electromagenetic torque (N.m)
V_s : Stator voltage (V)
V_r : rotor voltage (V)
V_{sd} : direct component of V_s in dq reference
V_{sq} : quadrature component of V_s in dq reference
V_{rd} : direct component of V_r in dq reference
V_{rq} : quadrature component of V_r in dq reference
i_{sd} : direct component of stator current
i_{sq} : quadrature component of stator current
ϕ_{sd} : direct component of stator flux
ϕ_{sq} : quadrature component of stator flux
i_{rd} : direct component of rotor current
i_{rq} : quadrature component of rotor current
P_s : Stator active power
Q_s : stator reactive power
i_{fd} : direct component of grid current
i_{fq} : quadrature component of grid current
P_f : rotor active power
i_{sd} : direct component of stator current
i_{sq} : quadrature component of stator current

Appendix

The WECS parameters used for the simulation are given in Tables 1, 2, 3 and 4.

Table 1. DFIG parameters

Parameter name	**Symbol**	**Value**	**Unit**
Rated power	P_n	1.5	MW
Rated voltage	U_n	690	V
Nominal frequency	f	50	Hz
Rated rotor speed	N	1750	rpm
number of pole pairs	p	2	
Stator resistance	R_s	2.65	mΩ
rotor resistance	R_r	2.63	mΩ
stator leakage inductance	$L_{s\sigma}$	0.1687	mH
rotor leakage inductance	$L_{r\sigma}$	0.1337	mH
magnetizing inductance	L_m	5.4749	mH

Table 2. The parameters of the turbine

Parameter name	**Symbol**	**Value**	**Unit**
Rated power	P_n	1.5	MW
Rated wind speed	v	13	m/s
Density of air	ρ	1,225	kg/m^3
Blade radius	R	30	m
Gearbox ratio	G	55	

Table 3. Parameters of the grid side

Parameter name	**Symbol**	**Value**	**Unit**
DC-link voltage	U_{dc}	1 200	V
DC-link capacitor	C	10 028.7	μF
filter resistance	R_f	0.3174	Ω
filter inductance	L_f	3.0103	mH

Table 4. Controller parameters

Parameter name	**Symbol**	**Value**
For rotor currents	K_p^r	0.8921
	K_i^r	7.8900
For grid currents	K_p^g	9.0309
	K_i^g	105.4380
For DC link voltage	K_p^{DC}	1.0029
	K_i^{DC}	50.1586

References

[1] IEA, *IEA (2021), Global Energy Review*, Paris (2021) Available at: https://www.iea.org/reports/global-energy-review-2021.

[2] Sen S., Ganguly S., *Opportunities, barriers and issues with renewable energy development – A discussion*, Renewable and Sustainable Energy Reviews, vol. 69, pp. 1170–1181 (2017), DOI: 10.1016/j.rser.2016.09.137.

[3] Li L. *et al.*, *Review and outlook on the international renewable energy development*, Energy and Built Environment (2020), DOI: 10.1016/j.enbenv.2020.12.002.

[4] Tawfiq K.B., Mansour A.S., Ramadan H.S., Becherif M., El-kholy E.E., *Wind Energy Conversion System Topologies and Converters: Comparative Review*, Energy Procedia, vol. 162, pp. 38–47 (2019), DOI: 10.1016/j.egypro.2019.04.005.

[5] Le T.-H., *A combined method for wind power generation forecasting*, Archives of Electrical Engineering, pp. 991-1009–991–1009 (2021), DOI: 10.24425/aee.2021.138274.

[6] Chen Z., Guerrero J.M., Blaabjerg F., *A Review of the State of the Art of Power Electronics for Wind Turbines*, IEEE Transactions on Power Electronics, vol. 24, no. 8, pp. 1859–1875 (2009), DOI: 10.1109/TPEL.2009.2017082.

[7] Mohammadi F. *et al.*, *Robust Control Strategies for Microgrids: A Review*, IEEE Systems Journal, vol. 16, no. 2, pp. 2401–2412 (2022), DOI: 10.1109/JSYST.2021.3077213.

[8] Aazami R., Heydari O., Tavoosi J., Shirkhani M., Mohammadzadeh A., Mosavi A., *Optimal Control of an Energy-Storage System in a Microgrid for Reducing Wind-Power Fluctuations*, Sustainability, vol. 14, no. 10 (2022), DOI: 10.3390/su14106183.

[9] Iranmehr H. *et al.*, *Modeling the Price of Emergency Power Transmission Lines in the Reserve Market Due to the Influence of Renewable Energies*, Frontiers in Energy Research, vol. 9 (2022), DOI: 10.3389/fenrg.2021.792418.

[10] Karad S., Thakur R., *Recent Trends of Control Strategies for Doubly Fed Induction Generator Based Wind Turbine Systems: A Comparative Review*, Archives of Computational Methods in Engineering, vol. 28, no. 1, pp. 15–29 (2021), DOI: 10.1007/s11831-019-09367-3.

[11] Mouhi N.E. Essadki A., *Active and Reactive Power Control of DFIG used in WECS using PI Controller and Backstepping*, in 2017 International Renewable and Sustainable Energy Conference (IRSEC), pp. 1–6 (2017), DOI: 10.1109/IRSEC.2017.8477349.

[12] Nadour M., Essadki A., Nasser T., *Comparative Analysis between PI & Backstepping Control Strategies of DFIG Driven by Wind Turbine*, International Journal of Renewable Energy Research, vol. 7, no. 3, pp. 1307–1316 (2017), DOI: 10.20508/ijrer.v7i3.6066.g7163.

[13] Mensou S., Essadki A., Minka I., Nasser T., Idrissi B.B., *Backstepping Controller for a Variable Wind Speed Energy Conversion System Based on a DFIG*, International Journal of Electrical and Computer Engineering, vol. 12, no. 9, pp. 598–604 (2018), DOI: 10.1109/IRSEC.2017.8477586.

[14] Barambones O., *Sliding Mode Control Strategy for Wind Turbine Power Maximization*, Energies, vol. 5 (2012), DOI: 10.3390/en5072310.

[15] Chakib R., Essadki A., Cherkaoui M., *Active Disturbance Rejection Control for Wind System Based on a DFIG*, International Journal of Electrical and Computer Engineering, vol. 8, no. 8, pp. 1313–1322 (2014), DOI: 10.5281/zenodo.1096099.

[16] Jabal Laafou A., Ait Madi A., Addaim A., Intidam A., *Dynamic Modeling and Improved Control of a Grid-Connected DFIG Used in Wind Energy Conversion Systems*, Mathematical Problems in Engineering, vol. 2020, p. e1651648 (2020), DOI: 10.1155/2020/1651648.

[17] Moumani Y., Laafou A.J., Ait Madi A., *Modeling and Backstepping Control of DFIG used in Wind Enegry Conversion System*, in 2021 7th International Conference on Optimization and Applications (ICOA), pp. 1–6 (2021), DOI: 10.1109/ICOA51614.2021.9442625.

[18] Fdaili M., Essadki A., Nasser T., *Comparative Analysis Between Robust SMC & Conventional PI Controllers Used in WECS Based on DFIG*, International Journal of Renewable Energy Research (IJRER), vol. 7, no. 4, no. 4 (2017), DOI: 10.20508/ijrer.v7i4.6441.g7267.

[19] Laafou A.J., Ait Madi A., Addaim A., *Dynamic Control of DFIG used in Wind Power Production, based on PI regulator*, in 2020 IEEE 2nd International Conference on Electronics, Control, Optimization and Computer Science (ICECOCS), pp. 1–6 (2020), DOI: 10.1109/ICECOCS50124.2020.9314563.

[20] Bossoufi B., Karim M., Lagrioui A., Taoussi M., Ghamrasni M.E., *Backstepping Adaptive Control of DFIG-Generators for Variable-Speed Wind Turbines*, International Journal of Computers and Technology, vol. 12, no. 7 (2014), DOI: 10.24297/ijct.v12i7.3079.

[21] Arbaoui M., Essadki A., *Comparative Analysis of ADRC & PI Controllers Used in Wind Turbine System Driving a DFIG*, International Journal of Renewable Energy Research (IJRER), vol. 7, no. 4, (2017), DOI: 10.20508/ijrer.v7i4.6270.g7225.